Symmetry-adapted calculations of strain and polarization fields in (111)-oriented zinc-blende quantum dots

S. Schulz,[1] M. A. Caro,[1,2] E. P. O'Reilly,[1,2] and O. Marquardt[1]
[1]*Photonics Theory Group, Tyndall National Institute, Lee Maltings, Cork, Ireland*
[2]*Department of Physics, University College Cork, Cork, Ireland*
(Received 10 May 2011; revised manuscript received 21 July 2011; published 13 September 2011)

We present expressions for the elastic and first-order piezoelectric tensor in (111)-oriented III-V zinc-blende semiconductors. Moreover, an equation for the second-order piezoelectric polarization vector in these systems is derived. Together these expressions provide an efficient route to calculate built-in potentials and strain fields in (111)-oriented zinc-blende nanostructures. Our detailed analysis provides insight into the key parameters that modify strain and built-in fields in a (111)-oriented zinc-blende system compared to a conventional (001) structure. We show that the calculated strain field in a (111)-oriented quantum dot displays the correct C_{3v} symmetry of the underlying crystal structure, even though we use a continuum-based approach and the quantum dot geometry is higher in symmetry than C_{3v}, e.g., $C_{\infty v}$. This behavior originates from an in-plane angle dependence of certain elastic tensor components in the (111)-zinc-blende system. In addition, we compare the elastic and the first-order piezoelectric tensor of the (111)-zinc-blende systems with the corresponding quantities in a wurtzite structure and point out similarities and differences. This comparison provides, for example, insight into the sign of the shear piezoelectric coefficient e_{15} in the wurtzite system, which is still under debate in the literature. Our analysis indicates $e_{15} < 0$, in accordance with recent experimental and theoretical results.

DOI: 10.1103/PhysRevB.84.125312 PACS number(s): 68.65.Hb, 77.22.Ej, 77.65.Ly, 77.65.Bn

I. INTRODUCTION

Over the last few years semiconductor quantum dots (QDs) have attracted considerable interest due to a variety of reasons,[1,2] including their potential in generating entangled photon pairs,[3,4] which are of high interest for use in novel quantum logical devices.[5–7] In general, conventional III-V QDs grown along the [001] direction do not allow for such entangled photons due to a nonzero fine-structure splitting (FSS) originating from the symmetry of the underlying zinc-blende (ZB) lattice and the related polarization potentials.[8,9] Reducing this FSS using post-growth thermal and laser annealing[10,11] is so far beyond the capabilities of industrial-scale production mechanisms of such QDs. Singh and Bester[12] and Schliwa *et al.*[13] therefore focused on ZB QDs grown on (111)-oriented substrates[14–17] and demonstrated that these systems, in principle, exhibit the required symmetry to achieve a zero FSS.[13] Recently grown site-controlled (111)-oriented InGaAs-QDs are most promising candidates to achieve a zero FSS.[17,18] They exhibit a flat, tetragonal shape with an extremely small ratio between dot height h and base length b ($h/b \sim 1/20$).[16,18,19] Certainly these QD systems can, for example, be addressed in terms of the conventional continuum elasticity theory and $\mathbf{k}\cdot\mathbf{p}$ models that are formulated to provide a good description of systems oriented along the [001] axis. However, due to the structural properties of the considered (111)-oriented ZB QDs, a high cell discretization is required to describe strain fields, built-in potentials, and electronic and optical properties of these large nanostructure systems accurately. When using a (001)-oriented cell, the QD growth axis is placed along the diagonal of the box and the size of the supercell has to be increased considerably to avoid numerical artifacts arising from the boundary conditions. In this case, the (001)-based description is less than ideal, both because of computing resource demands and also for clarity of interpretation.

In order to achieve higher efficiency of the calculations and a deeper insight into the key parameters that determine the elastic and polarization characteristics and finally the electronic and optical properties of (111)-oriented ZB QDs, it can be useful to work with a basis where the [111] direction is chosen as one of the coordinate axes. We present here the results of using such a basis, modifying the widely used expressions and codes based on using the conventional (001)-oriented continuum models by transforming to a (111)-oriented system. Here we derive expressions for the stiffness tensor, the elastic energy, and (first- and second-order) piezoelectric polarization vectors in (111)-oriented ZB structures. In the framework of continuum elasticity theory we calculate the strain and piezoelectric fields in (111)-oriented InGaAs/GaAs QDs. We show and discuss here that the calculated fields in these systems exhibit a C_{3v} symmetry even though neither the QD geometry nor the surrounding cell exhibit this specific symmetry.

Our approach has the additional benefit to gain further insights into some of the material parameters of c-plane wurtzite (WZ) systems, due to structural similarities to the (111)-oriented ZB systems. Even though the progress in epitaxial growth over the last few years has improved the quality of nitride-based heterostructures, some of the key material parameters are still not well known. For example, the sign of the shear piezoelectric coefficient e_{15}, which does not contribute to the built-in field in c-plane quantum wells but is important for QDs[20,21] and semipolar structures,[22] is surrounded by controversy. For example, Refs. 23–25 predict a positive sign, while Refs. 26–28 find a negative sign of e_{15}. From our previous analysis[29] of the built-in potential in nonpolar nitride-based GaN/AlN QDs, we concluded that e_{15} has to be negative to give a built-in field reduction in nonpolar GaN/AlN QDs compared to conventional c-plane systems, as observed experimentally.[30] Here, we show that by comparing the first-order piezoelectric tensor in the (111)-ZB system to

the tensor in the (0001)-WZ structure, this conclusion is further supported. Beyond that, we use the ZB-WZ comparison to point out both analogies and differences between these two systems.

The outline of the paper is as follows. Section II provides a detailed comparison of WZ and ZB structures, which allows us to identify similarities and differences between the two systems. In Sec. III we derive expressions for the elastic tensor and the elastic energy in (111)-oriented ZB systems. The findings are discussed with respect to conventional (001)-ZB systems and (0001)-WZ structures. The analysis is then extended to the study of strain fields in InGaAs QDs. In Sec. IV we focus on the symmetry adapted formulation of first- and second-order piezoelectric polarization vectors in (111)-oriented ZB structures. The resulting expressions are compared to WZ-like systems. Moreover, the influence of the different contributions in the polarization vector on the corresponding built-in potential in (111)-oriented InGaAs QDs is presented and discussed in this section. Finally we summarize and present our conclusions in Sec. V.

II. COMPARISON OF WURTZITE AND ZINC-BLENDE LATTICE

In this section, we focus our attention on the differences and similarities of ZB and WZ crystal structures. As discussed by Yeh *et al.*[31] the subtle disparities in the structural properties and the small differences in the internal energies lead to the situation that several binary semiconductors can crystallize in either form.

The Bravais lattice of the WZ system is hexagonal-closed-packed (hcp), while the Bravais lattice of the ZB structure is face-centered-cubic (fcc). The ZB structure consists of two interpenetrating fcc lattices, each with one type of atom, offset by one-quarter of the distance of a body diagonal, while the WZ structure can be thought of as two interpenetrating hcp lattices offset along the c axis by 5/8 of the cell height ($5c/8$).

The differences of the two systems is best understood when looking at the ZB structure along the [111] direction and at the WZ system along the c axis ([0001] direction). This is schematically shown in Figs. 1(a) and 1(b), respectively. Here, we find that the ZB and WZ structures look very similar and layers of atoms are arranged in regular hexagons. This hexagonal symmetry of the atoms within each layer leads to a C_{3v} symmetry for both ZB as well as WZ systems. Even though the atoms are identical within each layer, and the layers alternate between anions and cations, the structures show a different layer stacking sequence along the [111] direction. The stacking sequence for WZ is $ABABAB\ldots$, while for ZB it is $ABCABCABC\ldots$. These stacking sequences are referred to as the dihedral conformation,[31] which is said to be staggered for ZB and eclipsed for WZ [cf. Figs. 1(c) and 1(d), respectively]. In both crystal structures, the bonding of the nearest-neighbor atoms has a tetrahedral symmetry. The nearest-neighbor environment is therefore identical in the two structures. Nine of the twelve second nearest neighbors are also in identical positions. The other three second nearest neighbors are rotated by $\pi/3$ ZB with respect to their position in WZ.

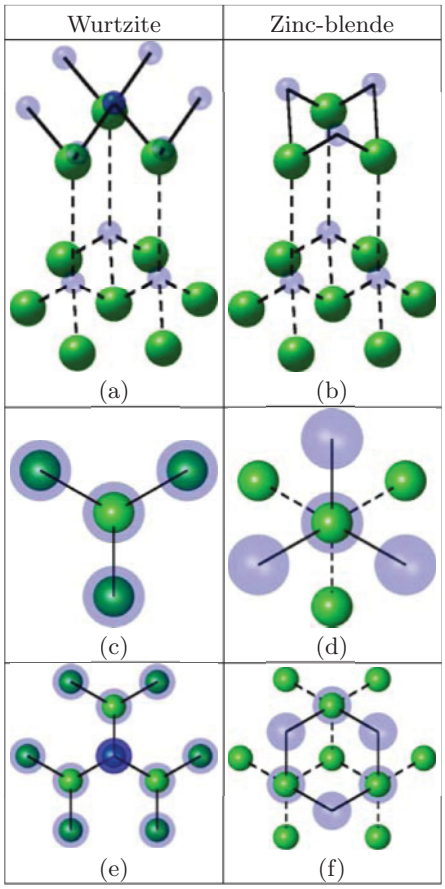

FIG. 1. (Color online) (a) Wurtzite and (b) zinc-blende crystal structures. In the wurtzite structure the c axis is pointing along the z direction while the z direction in the zinc-blende system shown is parallel to the [111] direction. The "eclipsed" and "staggered" dihedral conformations for wurtzite and zinc-blende are displayed in (c) and (d), respectively. The top view of c-plane wurtzite and (111)-oriented zinc-blende, indicating the layer to layer stacking along these directions, is shown in (e) and (f), respectively.

The differences between ZB and WZ are therefore only minor up to second nearest neighbors, and only become more marked for third and more distant neighbors. Due to these structural similarities, the transferability of parameters between the two polytypes is expected to be valid.

To gain further useful insights in the similarities and differences of WZ and ZB systems we focus in a second step on the point groups of the two polytypes. The point group of ZB semiconductors is T_d and contains 24 elements.[32] These elements include the identity, eight rotations of $2\pi/3$ (C_3) about $[\pm1,\pm1,\pm1]$, and three rotations of π (C_2) about the three mutually perpendicular crystallographic axes. Moreover, there are six improper rotations of $\pm\pi/2$ (S_4) and six reflections which leave the crystal invariant.[32]

The point group of a WZ crystal is C_{6v}.[32] This group has 12 elements which leave the crystal invariant. These elements are the identity, rotations of $\pm2\pi/3$ (C_3) around the c axis, three reflections in the vertical planes that contain the c axis and the reciprocal-lattice vectors, and six rotations, each followed by a translation of $[0,0,c/2]$.[32] Note also that inversion is not a symmetry operation.

If we focus our attention now on the description of ZB and WZ nanostructures, these symmetries will be further reduced. In the case of conventional (001)-oriented III-V ZB semiconductors (InAs/GaAs) the T_d point group symmetry is reduced to C_{2v} in realistic QD geometries,[33,34] since the rotoinversion (S_4) is no longer a symmetry operation which leaves the system invariant. This reduction in symmetry gives rise to a significant FSS in (001)-oriented InGaAs/GaAs QDs.[9,12]

In the case of (0001)-WZ QDs with realistic shapes (hexagonal truncated pyramids,[35] lens-shaped structures[36]) the C_{6v} point group symmetry is reduced to C_{3v}, lacking the six rotations that are followed by a translation of $[0,0,c/2]$.[34] As discussed by Singh *et al.*,[12] QD structures with perfect C_{3v} symmetry forbid a FSS.

When growing InGaAs/GaAs on (111)-oriented substrates, following our discussion above, one is also left with the same C_{3v} symmetry, explaining the recently measured[17,18] and calculated[12,13] vanishing FSS in these systems.

III. STRAIN FIELD IN QUANTUM DOT STRUCTURES

The aim of this section is to provide expressions for the stiffness (elastic) tensor and the elastic energy in (111)-oriented ZB systems, using a basis where the (111) direction is chosen as one of the coordinate axes. In the framework of a continuum-based approach, this then allows for an efficient calculation of the strain field in such a system. Furthermore, we will point out both the similarities and differences between the strain field in a (111)-oriented ZB QD and an otherwise identical c-plane WZ QD.

In semiconductor heterostructures, the lattice constant is position dependent. The total elastic energy of the system is given in a second-order continuum elasticity formulation by[37]

$$F = \frac{V}{2} \sum_{i,j,k,l} C_{ijkl}\epsilon_{ij}\epsilon_{kl}, \tag{1}$$

where V is the total volume of the system, ϵ_{ij} denotes the different components of the strain tensor, while C_{ijkl} are the components of the stiffness tensor. The indices i,j,k,l run over the spatial coordinates x, y, and z. Note that $\epsilon_{ij}(\mathbf{r})$ and $C_{ijkl}(\mathbf{r})$ are coordinate dependent for heterostructures. The strain tensor components ϵ_{ij} are commonly written as[38,39]

$$\epsilon_{ij}(\mathbf{r}) = \epsilon^{\mathbf{u}}_{ij}(\mathbf{r}) + \epsilon^{0}_{ij}(\mathbf{r}), \tag{2}$$

where $\epsilon^{0}_{ij}(\mathbf{r})$ is the local intrinsic strain and $\epsilon^{\mathbf{u}}_{ij}(\mathbf{r})$ denotes local strain arising from the displacement field $\mathbf{u}(\mathbf{r})$. The local strain tensor components $\epsilon^{\mathbf{u}}_{ij}(\mathbf{r})$ are defined by[37]

$$\epsilon^{\mathbf{u}}_{ij}(\mathbf{r}) = \frac{1}{2}\left(\frac{\partial u_i(\mathbf{r})}{\partial x_j} + \frac{\partial u_j(\mathbf{r})}{\partial x_i}\right). \tag{3}$$

For a given structure, the elastic energy F, Eq. (1), is minimized with respect to the displacement vector field $\mathbf{u}$.[38] Once the displacement field is known at each point, the position dependent strain field can be obtained from Eq. (3).

This continuum-based approach to calculate the strain field in a heterostructure does not capture the underlying atomistic structure. As discussed in detail in Ref. 40, in the framework of a continuum-based scheme the symmetry of a pyramidal-shaped (001)-oriented InAs/GaAs QD is C_{4v}, while an atomistic calculation gives the correct C_{2v} symmetry.[33,40] Reference 40 illustrates this artificial reduction of the system's symmetry for this specific QD, where a continuum elasticity model yields equal strains along the [110] and the $[\bar{1}10]$ directions, that are found to be different when employing an atomistic model, where the correct symmetry of the system is reproduced. However, since our main focus is on (111)-oriented ZB structures, we will show that in this case the continuum ansatz is sufficient to capture the correct symmetry of the system, namely the C_{3v} symmetry.

To analyze differences and similarities in the elastic properties of ZB and WZ systems we proceed in the following way: In Secs. III A and III B we briefly revisit the elastic tensor and the elastic energy of conventional (001)-ZB and (0001)-WZ systems, respectively. Expression for these quantities in (111)-oriented ZB systems are then derived and analyzed in Sec. III C.

A. Stiffness tensor and elastic energy in (001)-oriented zinc-blende structures

In (001)-oriented ZB structures one is left with only three independent elastic constants, which are given in Voigt notation as $C_{1111} = C_{11}$, $C_{1122} = C_{12}$, and $C_{1212} = C_{44}$. The stiffness tensor $C^{\mathrm{ZB}}_{(001)}$ takes the form[41]

$$C^{\mathrm{ZB}}_{(001)} = \begin{pmatrix} C_{11} & C_{12} & C_{12} & 0 & 0 & 0 \\ C_{12} & C_{11} & C_{12} & 0 & 0 & 0 \\ C_{12} & C_{12} & C_{11} & 0 & 0 & 0 \\ 0 & 0 & 0 & C_{44} & 0 & 0 \\ 0 & 0 & 0 & 0 & C_{44} & 0 \\ 0 & 0 & 0 & 0 & 0 & C_{44} \end{pmatrix}. \tag{4}$$

According to Eq. (1) the elastic energy $F^{(001)}_{\mathrm{ZB}}$ in a ZB structure using the standard coordinate system then reads

$$F^{(001)}_{\mathrm{ZB}} = \frac{V}{2}\left[C_{11}\left(\epsilon^2_{11} + \epsilon^2_{22} + \epsilon^2_{33}\right) + 2C_{12}(\epsilon_{11}\epsilon_{22} + \epsilon_{11}\epsilon_{33} + \epsilon_{22}\epsilon_{33}) + 4C_{44}(\epsilon^2_{12} + \epsilon^2_{13} + \epsilon^2_{23})\right]. \tag{5}$$

The local intrinsic strain ϵ^0_{ij} in a QD system is then given by

$$\epsilon^0_{ij} = \delta_{ij}\left[\frac{a_B - a(\mathbf{r})}{a(\mathbf{r})}\right]. \tag{6}$$

Here, a_B is the lattice constant of the barrier material. The position dependent lattice constant $a(\mathbf{r})$ is the lattice constant of the nanostructure material if $\mathbf{r}$ lies inside the nanostructure, otherwise $a(\mathbf{r}) = a_B$.

B. Stiffness tensor and elastic energy in (0001)-oriented wurtzite structures

In (0001)-oriented WZ structures, one is left with five independent elastic constants, namely $C^{\mathrm{WZ}}_{1111} = C^{\mathrm{WZ}}_{11}$, $C^{\mathrm{WZ}}_{3333} = C^{\mathrm{WZ}}_{33}$, $C^{\mathrm{WZ}}_{1122} = C^{\mathrm{WZ}}_{12}$, $C^{\mathrm{WZ}}_{1133} = C^{\mathrm{WZ}}_{13}$, and $C^{\mathrm{WZ}}_{1212} = C^{\mathrm{WZ}}_{44}$ and the

stiffness tensor takes the form:[41]

$$C^{\mathrm{wz}}_{(0001)} = \begin{pmatrix} C^{\mathrm{wz}}_{11} & C^{\mathrm{wz}}_{12} & C^{\mathrm{wz}}_{13} & 0 & 0 & 0 \\ C^{\mathrm{wz}}_{12} & C^{\mathrm{wz}}_{11} & C^{\mathrm{wz}}_{13} & 0 & 0 & 0 \\ C^{\mathrm{wz}}_{13} & C^{\mathrm{wz}}_{13} & C^{\mathrm{wz}}_{33} & 0 & 0 & 0 \\ 0 & 0 & 0 & C^{\mathrm{wz}}_{44} & 0 & 0 \\ 0 & 0 & 0 & 0 & C^{\mathrm{wz}}_{44} & 0 \\ 0 & 0 & 0 & 0 & 0 & C^{\mathrm{wz}}_{66} \end{pmatrix}. \quad (7)$$

with $C^{\mathrm{WZ}}_{66} = \frac{1}{2}(C^{\mathrm{wz}}_{11} - C^{\mathrm{wz}}_{12})$ and where the z axis is chosen along the [0001], c axis, direction. From Eq. (1), the elastic energy $F^{(0001)}_{\mathrm{wz}}$ in a WZ system is then given by

$$\begin{aligned} F^{(0001)}_{\mathrm{wz}} = \frac{V}{2}\big[& C^{\mathrm{wz}}_{11}\big(\epsilon^2_{11} + \epsilon^2_{22}\big) + C^{\mathrm{wz}}_{33}\epsilon^2_{33} + 2C^{\mathrm{wz}}_{12}\epsilon_{11}\epsilon_{22} \\ & + 2C^{\mathrm{wz}}_{13}\epsilon_{33}(\epsilon_{11} + \epsilon_{22}) + 4C^{\mathrm{wz}}_{44}\big(\epsilon^2_{13} + \epsilon^2_{23}\big) \\ & + 2\big(C^{\mathrm{wz}}_{11} - C^{\mathrm{wz}}_{12}\big)\epsilon^2_{12}\big]. \end{aligned} \quad (8)$$

For a WZ nanostructure embedded in a WZ matrix of a different material with lattice constants a_B and c_B, the local intrinsic strain ϵ^0_{ij} is given by

$$\epsilon^0_{ij} = (\delta_{ij} - \delta_{i3}\delta_{j3})\left[\frac{a_B - a(\mathbf{r})}{a(\mathbf{r})}\right] + \delta_{i3}\delta_{j3}\left[\frac{c_B - c(\mathbf{r})}{c(\mathbf{r})}\right]. \quad (9)$$

The position dependent lattice constant $a(\mathbf{r})$ $[c(\mathbf{r})]$ is the lattice constant of the nanostructure material if $\mathbf{r}$ lies inside the nanostructure, otherwise $a(\mathbf{r}) = a_B$ $[c(\mathbf{r}) = c_B]$.

C. Stiffness tensor and elastic energy in (111)-oriented zinc-blende structures

The stiffness tensor for an arbitrary basis vector orientation can be obtained using a rotation matrix of the form

$$U = \begin{pmatrix} \cos\theta\cos\phi & \cos\theta\sin\phi & -\sin\theta \\ -\sin\phi & \cos\phi & 0 \\ \sin\theta\cos\phi & \sin\theta\sin\phi & \cos\theta \end{pmatrix}. \quad (10)$$

The rotation with the Euler angles, as shown in Fig. 2, transforms vectors and tensors from (x,y,z) to (x',y',z') coordinates via the expressions[45]

$$P'_i = \sum_\alpha U_{i\alpha} P_\alpha, \quad (11)$$

$$\epsilon'_{ij} = \sum_{\alpha,\beta} U_{i\alpha}U_{j\beta}\epsilon_{\alpha\beta}, \quad (12)$$

$$C'_{ijkl} = \sum_{\alpha,\beta,\gamma,\delta} U_{i\alpha}U_{j\beta}U_{k\gamma}U_{l\delta}C_{\alpha\beta\gamma\delta}, \quad (13)$$

where $i,j,k,l,\alpha,\beta,\gamma,\delta = 1,2,3 \equiv x,y,z$.

Here, to obtain the (111)-oriented ZB stiffness tensor $C^{\mathrm{ZB}}_{(111)}$, we substitute $\cos\theta = 1/\sqrt{3}$, $\sin\theta = \sqrt{2/3}$, and

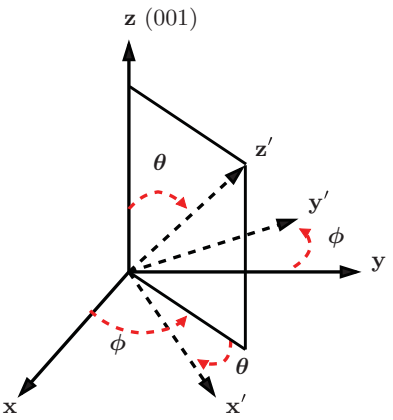

FIG. 2. (Color online) Configuration of the coordinate system (x',y',z') in (hkl)-oriented crystals. The growth axis z' is normal to the substrate surface (hkl). The coordinate system (x,y,z) denotes the primary crystallographic axes. The Euler angles θ and ϕ are the polar azimuthal angles of the direction z' in terms of the (x,y,z) coordinates.

$\cos\phi = \sin\phi = 1/\sqrt{2}$ into Eq. (10) and use Eq. (13) to rotate $C^{\mathrm{ZB}}_{(001)}$ to the (111)-oriented coordinate system. This yields

$$C^{\mathrm{ZB}}_{(111)} = \begin{pmatrix} C'_{11} & C'_{12} & C'_{13} & 0 & C'_{15} & 0 \\ C'_{12} & C'_{11} & C'_{13} & 0 & -C'_{15} & 0 \\ C'_{13} & C'_{13} & C'_{33} & 0 & 0 & 0 \\ 0 & 0 & 0 & C'_{44} & 0 & -C'_{15} \\ C'_{15} & -C'_{15} & 0 & 0 & C'_{44} & 0 \\ 0 & 0 & 0 & -C'_{15} & 0 & C'_{66} \end{pmatrix} \quad (14)$$

with

$$\begin{aligned} C'_{11} &= \frac{1}{2}(C_{11} + C_{12}) + C_{44}, \\ C'_{33} &= \frac{3}{2}C'_{11} - \frac{1}{2}C'_{12} - C'_{44}, \\ C'_{44} &= \frac{1}{3}(C_{11} - C_{12}) + \frac{1}{3}C_{44}, \\ C'_{12} &= \frac{1}{6}(C_{11} + 5C_{12}) - \frac{1}{3}C_{44}, \\ C'_{13} &= -\frac{1}{2}C'_{11} + \frac{3}{2}C'_{12} + C'_{44}, \\ C'_{15} &= \frac{1}{\sqrt{2}}C'_{11} - \frac{1}{\sqrt{2}}C'_{12} - \sqrt{2}C'_{44}, \\ C'_{66} &= \frac{1}{2}(C'_{11} - C'_{12}). \end{aligned} \quad (15)$$

Similarly to the (001)-ZB system we are left with three independent elastic constants. These expressions are equivalent to the results found by Martin[46] and used in Ref. 47 to calculate elastic constants of cubic III-N semiconductors. In order to study how the subtle differences, discussed in Sec. II, of WZ and ZB structures affect the transferability of parameters between those two systems, we focus in a first step on the elastic constants. Here, we calculate the elastic constants C'_{ij} in the (111)-ZB system from the (001)-ZB ones,

TABLE I. Elastic constants C_{ij} for InN, GaN and AlN. The values for the elastic constants in (111)-oriented zinc-blende system [(111)-ZB] are calculated according to Eqs. (15).

	InN			GaN			AlN		
	(001)-ZB	(111)-ZB	(0001)-WZ	(001)-ZB	(111)-ZB	(0001)-WZ	(001)-ZB	(111)-ZB	(0001)-WZ
C_{11} (GPa)	185[a]	226	223,[b] 227[c]	297[a]	367	390,[b] 347[c]	314[a]	393	396,[b] 390[c]
C_{33} (GPa)		240	224,[b] 245[c]		388	398,[b] 396[c]		419	373,[b] 375[c]
C_{44} (GPa)	80[a]	53	48,[b] 52[c]	154[a]	108	105,[b] 99[c]	200[a]	105	116,[b] 127[c]
C_{66} (GPa)		67	54,[b] 55[c]		132	123,[b] 104[c]		131	130,[b] 129[c]
C_{12} (GPa)	107[a]	93	115,[b] 118[c]	126[a]	103	145,[b] 139[c]	157[a]	131	137,[b] 133[c]
C_{13} (GPa)		80	92,[b] 98[c]		80	106,[b] 105[c]		105	108,[b] 103[c]
C_{15} (GPa)		19			73			37	

[a]Reference 42.
[b]Reference 43.
[c]Reference 44.

C_{ij}, using Eqs. (15). The values for the ZB elastic constants C_{ij} of cubic GaN, AlN, and InN are taken from Ref. 42. The resulting elastic constants C'_{ij} are compared to literature values of WZ GaN, AlN, and InN in Table I. We find that the agreement between the calculated (111)-ZB values and the values taken from the literature for the WZ system is surprisingly good for the diagonal components C_{ii} in InN and GaN. The agreement is still acceptable for the off-diagonal terms C_{12} and C_{13} in these systems. The agreement is also very good for four of the elastic constants in AlN, and acceptable for the remaining two constants, C_{33} and C_{44}. Therefore since the overall agreement is good, this further suggests that the (111)-ZB approximation for the WZ parameters is a reasonable assumption. The major difference between the two systems in terms of elastic constants is the contribution C'_{15}, which is missing in a (0001)-oriented WZ structure. We show in the Appendix that this additional elastic tensor component exhibits a threefold (C_{3v}) symmetry. This C_{3v} symmetry becomes visible when calculating the strain tensor components ϵ_{ij} in a (111)-oriented ZB QD structure. Using Eq. (1), the elastic energy $F_{\mathrm{ZB}}^{(111)}$ in the (111)-oriented ZB system is given by

$$F_{\mathrm{ZB}}^{(111)} = \frac{V}{2}\left[C'_{11}\left(\epsilon_{11}^2+\epsilon_{22}^2\right)+C'_{33}\epsilon_{33}^2+2C'_{12}\epsilon_{11}\epsilon_{22}\right.$$
$$+2C'_{13}\epsilon_{33}(\epsilon_{11}+\epsilon_{22})+4C'_{44}\left(\epsilon_{13}^2+\epsilon_{23}^2\right)$$
$$+2(C'_{11}-C'_{12})\epsilon_{12}^2+4C'_{15}\epsilon_{13}(\epsilon_{11}-\epsilon_{22})$$
$$\left.-8C'_{15}\epsilon_{12}\epsilon_{23}\right]. \qquad (16)$$

The major difference in this expression compared to that for the elastic energy of a WZ system, Eq. (8), arises from the terms related to C'_{15}. By minimizing the elastic energy with respect to the displacement vector field $\mathbf{u}(\mathbf{r})$ and using Eq. (3), we obtain the corresponding strain tensor components ϵ_{ij}. As a model system we have chosen here a lens-shaped QD, which exhibits a $C_{\infty v}$ symmetry. Hence the symmetry of the strain field is determined by the symmetry properties of the elastic tensor. In the case of a lens-shaped (001)-ZB QD or (0001)-WZ QD the elastic constants C_{ij} do not show any angle dependence in the growth plane. Consequently, the continuum-based strain field "sees" the QD shape only. If we neglect the C'_{15} terms in the elastic energy $F_{\mathrm{ZB}}^{(111)}$, Eq. (16), of the (111)-oriented ZB system, we are left with the elastic energy of a c-plane WZ system, Eq. (8). To study the influence of the C'_{15} terms on the strain field, we have compared the results of the WZ-like approximation with those obtained from Eq. (16), taking C'_{15} terms into account. As a model system we have chosen a lens-shaped $In_{0.35}Ga_{0.65}As$/GaAs QD with a base length of 13 nm and a height of 3 nm. All calculations were performed using the S/PHI/nX software library.[48–50] The relevant material parameters are summarized in Table II. The calculated hydrostatic strain, $\mathrm{Tr}(\boldsymbol{\epsilon})$, in the $x-y$ plane, 0.5 nm above the QD base, is shown in Fig. 3. The lower half of the figure displays $\mathrm{Tr}(\boldsymbol{\epsilon})$ in the WZ-like approximation ($C'_{15}=0$) while the upper half shows the results from the full calculation ($C'_{15}\neq 0$). As expected from our discussion above, the WZ-like approximation leads to a strain field that exhibits a $C_{\infty v}$ symmetry, since the chosen QD geometry has this symmetry. This has to be contrasted with the calculated hydrostatic strain obtained from the complete (111)-ZB expression for the elastic energy, Eq. (16), shown in the upper half of Fig. 3. Since the elastic tensor $C_{(111)}^{\mathrm{ZB}}$ has an in-plane angle dependence, $\mathrm{Tr}(\boldsymbol{\epsilon})$ exhibits a C_{3v} symmetry, even though we are using a classic harmonic continuum-elasticity approach. Note that $\mathrm{Tr}(\boldsymbol{\epsilon})$ is shown in Fig. 3 for the same contour lines. It can

TABLE II. Material parameters for InAs and GaAs.

	GaAs	InAs
a (Å)	5.6503[a]	6.0553[a]
C_{11} (GPa)	118.8[b]	83.3[b]
C_{12} (GPa)	53.8[b]	45.3[b]
C_{44} (GPa)	59.4[b]	39.6[b]
ϵ_r	13.18[c]	14.6[c]
e_{14} (C/m^2)	−0.230[d]	−0.115[d]
B_{114} (C/m^2)	−0.439[d]	−0.531[d]
B_{124} (C/m^2)	−3.765[d]	−4.076[d]
B_{156} (C/m^2)	−0.492[d]	−0.120[d]
A_1 (C/m^2)	−2.656	−2.894
A_2 (C/m^2)	+2.217	+2.363

[a]Reference 51.
[b]Reference 52.
[c]Reference 53.
[d]Reference 54.

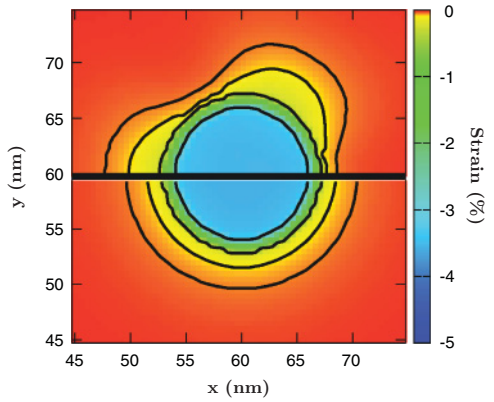

FIG. 3. (Color online) Contour plots of the hydrostatic strain [Tr(ϵ)] in (111)-oriented lens-shaped $In_{0.35}Ga_{0.65}As/GaAs$ QDs. The lens-shaped QD has a base length of $b = 13$ nm and height of $h = 3$ nm. The lower half shows Tr(ϵ) in the WZ-like approximation, neglecting C'_{15} contributions in the elastic energy $F_{\mathrm{ZB}}^{(111)}$, Eq. (16), while the upper half displays Tr(ϵ) calculated from Eq. (16) including C'_{15} contributions.

be seen that the WZ-like description gives almost the same hydrostatic strain in and around the QD structure as the full ($C'_{15} \neq 0$) (111)-ZB description. Only in regions of small strain, Tr(ϵ) $< 1\%$, differences become more visible, but are still relatively small. Hence for this archetypal dot shape we find that there is little difference in the hydrostatic strain behavior between the WZ-like and full ZB cases.

IV. POLARIZATION FIELDS IN SEMICONDUCTOR NANOSTRUCTURES

Under applied stress, semiconductor materials with a lack of inversion symmetry show an electric polarization dependent on the applied stress.[55] This strain-induced polarization, referred to as the piezoelectric polarization, is described in general by the first-order piezoelectric tensor e_{ijk} (linear regime) plus possible higher-order terms, e.g., quadratic contributions B_{ijklm}, which are connected to the polarization vector $\mathbf{P}_{\mathrm{pz}}$ via the strain state of the system:[56]

$$P_{\mathrm{pz},i} = \sum_{jk} e_{ijk}\epsilon_{jk} + \frac{1}{2}\sum_{jklm} B_{ijklm}\epsilon_{jk}\epsilon_{lm} + \cdots . \quad (17)$$

Converting from tensor representation to matrix notation, the linear contribution in Eq. (17) takes the form

$$\begin{pmatrix} P_{\mathrm{pz},x} \\ P_{\mathrm{pz},y} \\ P_{\mathrm{pz},z} \end{pmatrix} = \begin{pmatrix} e_{11} & e_{12} & e_{13} & e_{14} & e_{15} & e_{16} \\ e_{21} & e_{22} & e_{23} & e_{24} & e_{25} & e_{26} \\ e_{31} & e_{32} & e_{33} & e_{34} & e_{35} & e_{36} \end{pmatrix} \begin{pmatrix} \epsilon_{11} \\ \epsilon_{22} \\ \epsilon_{33} \\ 2\epsilon_{23} \\ 2\epsilon_{13} \\ 2\epsilon_{12} \end{pmatrix}. \quad (18)$$

In contrast to the ZB system, the total polarization vector $\mathbf{P}_{\mathrm{tot}}$ in semiconductors with a WZ crystal structure arises from two contributions: the strain-related piezoelectric contribution $\mathbf{P}_{\mathrm{pz}}$ discussed above and the spontaneous polarization $\mathbf{P}_{\mathrm{sp}}$.[57]

The spontaneous polarization originates from the lack of inversion symmetry along the c axis ([0001] direction) in a WZ lattice.[58] Because of the crystal symmetry, $\mathbf{P}_{\mathrm{sp}}$ is a constant vector oriented along the c axis.

The charge density ρ_p arising from the polarization $\mathbf{P}_{\mathrm{tot}}$ is given by

$$\rho_p(\mathbf{r}) = -\nabla \cdot \mathbf{P}_{\mathrm{tot}}. \quad (19)$$

The corresponding electrostatic built-in potential ϕ_p is found, in the absence of external charges, by solving the Maxwell equation

$$\nabla \cdot \mathbf{D} = 0, \quad (20)$$

where the displacement vector $\mathbf{D}$ is given by

$$\mathbf{D} = -\varepsilon_0\varepsilon_s(\mathbf{r})\nabla\phi_p + \mathbf{P}_{\mathrm{tot}}. \quad (21)$$

The material dependent dielectric constant is denoted by $\varepsilon_s(\mathbf{r})$ and $\mathbf{P}_{\mathrm{tot}}$ is the total polarization vector of the system under consideration.

Please note that, in the present work, we focus our discussion on a non-self-consistent calculation of strain and piezoelectric potentials, i.e., we neglect the electric-field influence on the elastic energy in Eq. (1). This coupling between piezoelectric potentials and strain was previously found to have a strong influence on the strength of the piezoelectric potential in GaN/AlN-quantum wells (QWs),[59] but did not induce significant modifications in $In_{0.2}Ga_{0.8}N/GaN$ QWs[60] and, in particular, this self-consistent approach induces only minor, quantitative modifications in ZB $In_xGa_{1-x}As$ systems,[54] which are the main subject of the present work. Moreover, as both the elastic tensor and the piezoelectric potential reflect a C_{3v} symmetry, we do not expect the electromechanical coupling to induce qualitative, i.e., symmetry-breaking modifications. Furthermore, the aim of this work is to provide expressions/equations that allow for an efficient calculation of strain and built-in fields in (111)-oriented ZB heterostructures, rather than describing these systems quantitatively in all details. Therefore expanding our formulation of the elastic energy and the piezoelectric potentials to a self-consistent model that includes electromechanical coupling is beyond the scope of the present work.

A. First- and second-order piezoelectric polarization in (001)-zinc-blende structures

For (001)-oriented ZB crystals, the only nonvanishing coefficients in the piezoelectric tensor $e^{\mathrm{ZB}}_{(001)}$, Eq. (18), are $e_{14} = e_{25} = e_{36}$. Therefore $e^{\mathrm{ZB}}_{(001)}$ reads

$$e^{\mathrm{ZB}}_{(001)} = \begin{pmatrix} 0 & 0 & 0 & e_{14} & 0 & 0 \\ 0 & 0 & 0 & 0 & e_{14} & 0 \\ 0 & 0 & 0 & 0 & 0 & e_{14} \end{pmatrix}, \quad (22)$$

and the first-order piezoelectric polarization vector $\mathbf{P}^{(001),\mathrm{FO}}_{\mathrm{pz}}$ is given by

$$\mathbf{P}^{(001),\mathrm{FO}}_{\mathrm{pz}} = 2e_{14}\begin{pmatrix} \epsilon_{23} \\ \epsilon_{13} \\ \epsilon_{12} \end{pmatrix}. \quad (23)$$

Measurements of piezoelectric fields in (111)-grown InGaAs/GaAs QWs[61–63] indicated a nonlinear behavior of the piezoelectric polarization with increasing In concentration and therefore higher strains. Bester *et al.*[54] introduced and calculated second-order piezoelectric coefficients $B_{i\alpha\beta}$ (Voigt notation), Eq. (17), to explain these effects. Łepkowski[64] performed calculations (neglecting In segregation) on multiple InGaAs QWs, and found when using the approach introduced by Bester *et al.* a built-in field of 166 kV/cm. This value is in good agreement with the measured value of 165 kV/cm,[65] which, however, has been extracted from the measurements using a linear theory. Therefore the drawn conclusion is not necessarily conclusive. Migliorato *et al.*[66] proposed a different scheme to take nonlinearity effects into account. In this scheme, the linear piezoelectric coefficient e_{14} is strain dependent, leading to a good agreement with the experimental data provided.[66] Furthermore, Migliorato *et al.*[66] showed also that the second-order contributions introduced by Bester *et al.*[54] should give a piezoelectric field of 80 kV/cm and not 166 kV/cm as obtained in Ref. 64. A similar discussion of these issues is also given in the recent review article by Lew Yan Voon and Willatzen.[67] Given the disagreement on the theoretical description of nonlinear effects in piezoelectric fields, further theoretical and experimental work is required. This issue is beyond the scope of the present work. Since the approach of introducing second-order piezoelectric coefficients $B_{i\alpha\beta}$ has been widely used,[12,13,64,68–72] the aim here is to provide an expression for the second-order piezoelectric vector in a (111)-oriented ZB system based on Eq. (17). Such an expression facilitates then numerically efficient calculations.

In the case of a (001)-ZB system, the second-order piezoelectric tensor $B_{i\alpha\beta}$ has 24 nonzero elements, which can be reduced to three independent elements B_{114}, B_{124}, and B_{156}.[56] In order to partially simplify the transformation to the (111)-oriented ZB system, we write the second-order terms in a modified form, involving hydrostatic and biaxial strain terms. The modified polarization vector $\mathbf{P}_{\rm pz}^{(001),\rm SO}$ due to second-order piezoelectricity is obtained from Eq. (17) as

$$\mathbf{P}_{\rm pz}^{(001),\rm SO} = 2A_1\begin{pmatrix}\mathrm{Tr}(\epsilon)\epsilon_{23}\\ \mathrm{Tr}(\epsilon)\epsilon_{13}\\ \mathrm{Tr}(\epsilon)\epsilon_{12}\end{pmatrix} + 2A_2\begin{pmatrix}\epsilon_{B,x}\,\epsilon_{23}\\ \epsilon_{B,y}\,\epsilon_{13}\\ \epsilon_{B,z}\,\epsilon_{12}\end{pmatrix} + 4B_{156}\begin{pmatrix}\epsilon_{13}\epsilon_{12}\\ \epsilon_{23}\epsilon_{12}\\ \epsilon_{23}\epsilon_{13}\end{pmatrix}, \tag{24}$$

with $A_1 = \frac{1}{3}B_{114} + \frac{2}{3}B_{124}$ and $A_2 = \frac{2}{3}B_{114} - \frac{2}{3}B_{124}$. The A_1 term is related to the hydrostatic strain, $\mathrm{Tr}(\boldsymbol{\epsilon}) = \epsilon_{11} + \epsilon_{22} + \epsilon_{33}$, while the A_2 contribution is linked to the biaxial strain components $\epsilon_{B,x} = \epsilon_{11} - (1/2)(\epsilon_{22} + \epsilon_{33})$, $\epsilon_{B,y} = \epsilon_{22} - (1/2)(\epsilon_{11} + \epsilon_{33})$, and $\epsilon_{B,z} = \epsilon_{33} - (1/2)(\epsilon_{22} + \epsilon_{11})$. The contribution arising from B_{156} is given by products of shear strain components. Surprisingly, when looking at the coefficients A_1 and A_2, we find here that these coefficients are almost identical in magnitude (cf. Table II) even though they are related to very different strain states of the system. The similar magnitude of the second-order piezoelectric response to hydrostatic and biaxial strain is not obvious and merits further investigation.

We note also that the biaxial strain terms $\epsilon_{B,i}$, will, by symmetry, be equal to zero along the central [111] axis, while the hydrostatic strain, $\mathrm{Tr}(\boldsymbol{\epsilon})$ will be large inside the dot, and relatively small outside the dot. We can therefore expect, if A_1 and A_2 are of comparable magnitude, that the A_1 terms will make the greatest contribution to the corresponding second-order piezoelectric potential along the central axis of a symmetric dot. We shall see below that this is indeed the case.

B. Piezoelectric and spontaneous polarization in (0001)-wurtzite structures

In a system with a WZ crystal structure there are three independent piezoelectric coefficients e_{15}, e_{31}, and e_{33} in the first-order piezoelectric tensor $e_{(0001)}^{\rm WZ}$, Eq. (18). To distinguish the piezoelectric coefficients of the WZ system from the ZB ones, we indicate the WZ system by a tilde, e.g., $\tilde{e}_{15}$, $\tilde{e}_{31}$, and $\tilde{e}_{33}$. In the WZ system $e_{(0001)}^{\rm WZ}$ is given by

$$e_{(0001)}^{\rm WZ} = \begin{pmatrix}0 & 0 & 0 & 0 & \tilde{e}_{15} & 0\\ 0 & 0 & 0 & \tilde{e}_{15} & 0 & 0\\ \tilde{e}_{31} & \tilde{e}_{31} & \tilde{e}_{33} & 0 & 0 & 0\end{pmatrix}. \tag{25}$$

The first-order piezoelectric polarization vector $\mathbf{P}_{\rm pz}^{\rm WZ,FO}$ is given by

$$\mathbf{P}_{\rm pz}^{\rm WZ,FO} = \begin{pmatrix}2\tilde{e}_{15}\epsilon_{13}\\ 2\tilde{e}_{15}\epsilon_{23}\\ \tilde{e}_{31}(\epsilon_{11}+\epsilon_{22}) + \tilde{e}_{33}\epsilon_{33}\end{pmatrix}. \tag{26}$$

The spontaneous polarization vector $\mathbf{P}_{\rm sp}$ is a constant vector along the c axis (z direction), $\mathbf{P}_{\rm sp} = P_{\rm sp}\mathbf{e}_z$, where $\mathbf{e}_z$ is the unit vector along the z direction and $P_{\rm sp}$ is a material specific constant.

So far, second-order coefficients $B_{i\alpha\beta}$ for the piezoelectric polarization in WZ semiconductors have not been reported in the literature. Therefore the present analysis is restricted to the contributions of the first-order piezoelectricity and the spontaneous polarization.

C. First-order piezoelectric polarization in (111)-zinc-blende structures

To derive expressions for the first-order piezoelectric polarization vector $\mathbf{P}_{\rm pz}^{(111),\rm FO}$, we proceed in the following way. Using the transformation matrix U from Eq. (10), the components e'_{ijk} of the first-order piezoelectric tensor $e_{(111)}^{\rm ZB}$ are obtained from the components e_{ijk} of the piezoelectric tensor $e_{(001)}^{\rm ZB}$ via

$$e'_{ijk} = \sum_{\alpha,\beta,\gamma} U_{i\alpha}U_{j\beta}U_{k\gamma}e_{\alpha\beta\gamma}.$$

In Voigt notation, this transformation gives

$$e_{(111)}^{\rm ZB} = \begin{pmatrix}e'_{11} & e'_{12} & 0 & 0 & e'_{15} & 0\\ 0 & 0 & 0 & e'_{15} & 0 & e'_{12}\\ e'_{31} & e'_{31} & e'_{33} & 0 & 0 & 0\end{pmatrix}, \tag{27}$$

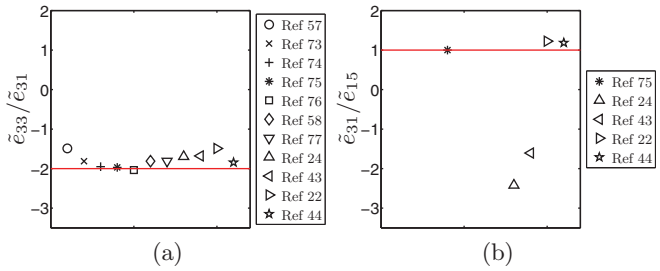

FIG. 4. (Color online) Ratio of the GaN piezoelectric coefficients (a) $\tilde{e}_{33}/\tilde{e}_{31}$ and (b) $\tilde{e}_{31}/\tilde{e}_{15}$. Our prediction, obtained from the (111)-ZB system, is given by the (red) solid line.

with $e'_{11} = -\sqrt{\frac{2}{3}}e_{14}$, $e'_{12} = \sqrt{\frac{2}{3}}e_{14}$, $e'_{15} = e'_{31} = -\frac{1}{\sqrt{3}}e_{14}$, and $e'_{33} = \frac{2}{\sqrt{3}}e_{14}$. Bernardini *et al.*[57] derived the same expressions for e'_{33} and e'_{31}. It was argued by the same authors that the direct comparison of the (111)-ZB system and the (0001)-WZ system is meaningful for two reasons: First, the possible deviations from the ideal WZ structure do not influence significantly the polarization derivatives (e.g., the piezoelectric coefficients),[57] and second, Dal Corso *et al.*[79] showed that in polytypical systems the values of the piezoelectric constants in the two competing structures agree within a few percent. Therefore we use the results obtained from the (111)-ZB system to gain insights into the piezoelectric coefficients of the WZ system. Figure 4 shows the ratios $\tilde{e}_{33}/\tilde{e}_{31}$ and $\tilde{e}_{31}/\tilde{e}_{15}$ for different sets of literature values for GaN, while Figs. 5 and 6 display these ratios for parameters sets for InN and AlN, respectively.[82]

When looking at the ratio $\tilde{e}_{33}/\tilde{e}_{31}$ we find that the agreement between the (111)-ZB approximation and the ratio calculated from the WZ literature values is very good for GaN and InN [cf. Figs. 4(a) and 5(a)]. This holds also for the ratio $\tilde{e}_{31}/\tilde{e}_{15}$, as long as the literature value for $\tilde{e}_{15}$ is negative [cf. Figs. 4(b) and 5(b)]. The agreement for the AlN system is less good, but still admissible for $\tilde{e}_{33}/\tilde{e}_{31}$ [cf. Fig. 6(a)]. The same is true for the ratio $\tilde{e}_{31}/\tilde{e}_{15}$ if $\tilde{e}_{15} < 0$, as shown in Fig. 6(b). The difference between AlN and the other two systems is that AlN exhibits a considerably larger crystal-field splitting than GaN and InN.[43] Furthermore, the crystal-field splitting is negative in the AlN system. To describe the crystal-field splittings accurately in the WZ system, interactions up to third nearest neighbors have to be taken into account, as discussed in detail in Ref. 83. The approach chosen here for the comparison between (111)-ZB and (0001)-WZ, however, assumes that these contributions are

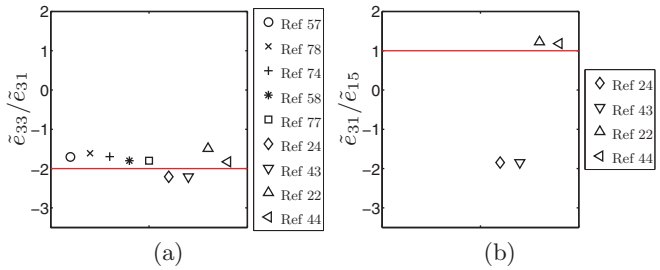

FIG. 5. (Color online) Ratio of the InN piezoelectric coefficients (a) $\tilde{e}_{33}/\tilde{e}_{31}$ and (b) $\tilde{e}_{31}/\tilde{e}_{15}$. Our prediction, obtained from the (111)-ZB system, is given by the (red) solid line.

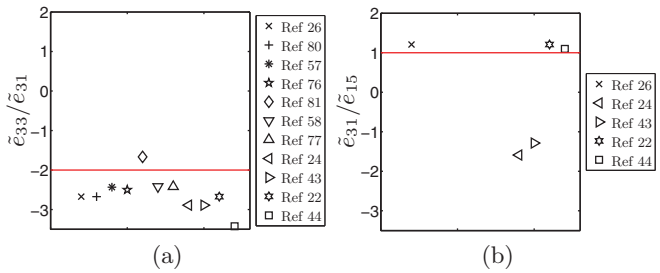

FIG. 6. (Color online) Ratio of the AlN piezoelectric coefficients (a) $\tilde{e}_{33}/\tilde{e}_{31}$ and (b) $\tilde{e}_{31}/\tilde{e}_{15}$. Our prediction, obtained from the (111)-ZB system, is given by the (red) solid line. In Ref. 81 only the piezoelectric strain/modulus component d_{33} was reported. We have used $d_{33} = -2d_{31}$ to determine d_{31} as suggested by the same authors.

negligible. Therefore this might explain why we find a better agreement between the (111)-ZB predictions and the ratios calculated from literature WZ values for GaN and InN than for AlN.

After this discussion on the general structure of the piezoelectric tensor we focus now on the related first-order built-in potential, investigating the effects of the differences in the strain and polarization vector components in a (111)-oriented ZB structure compared to an equivalent wurtzite system.

Comparing $e^{\mathrm{ZB}}_{(111)}$, Eq. (27), with the piezoelectric tensor $e^{\mathrm{WZ}}_{(0001)}$, Eq. (25), we observe that the lower symmetry of the (111)-ZB system (C_{3v} symmetry), with respect to the WZ crystal structure (C_{6v} symmetry), leads to additional terms in $e^{\mathrm{ZB}}_{(111)}$. Consequently, these contributions will also modify the first-order polarization vector $\mathbf{P}^{(111),\mathrm{FO}}_{\mathrm{pz}}$. When calculating $\mathbf{P}^{(111),\mathrm{FO}}_{\mathrm{pz}}$ from

$$P^{(111),\mathrm{FO}}_{\mathrm{pz,i}} = \sum_{jk} e'_{ijk}\epsilon'_{jk}, \tag{28}$$

we obtain

$$\mathbf{P}^{(111),\mathrm{FO}}_{\mathrm{pz}} = \begin{pmatrix} 2e'_{15}\epsilon'_{13} \\ 2e'_{15}\epsilon'_{23} \\ e'_{31}(\epsilon'_{11}+\epsilon'_{22}) + e'_{33}\epsilon'_{33} \end{pmatrix} + \begin{pmatrix} e'_{11}(\epsilon'_{11}-\epsilon'_{22}) \\ 2e'_{12}\epsilon'_{12} \\ 0 \end{pmatrix}, \tag{29}$$

where ϵ'_{ij} denote the strain tensor components in the (111)-ZB system.

We turn now to investigate the influence of the additional terms in the elastic energy, Eq. (16), and the piezoelectric tensor, Eq. (27), respectively, on the first-order built-in potential ϕ^{FO}_p in a (111)-oriented InGaAs/GaAs QD as compared to an equivalent WZ-like structure. As model system we choose again a lens-shaped $In_{0.35}Ga_{0.65}As$ QD with a base length of 13 nm and a height of 3 nm. To systematically study the different contributions to ϕ^{FO}_p, we start in a first step with a WZ-like approximation. To this end, we neglect the additional terms e'_{11} and e'_{12} in the piezoelectric tensor $e^{\mathrm{ZB}}_{(111)}$, Eq. (27), and the off-diagonal term C'_{15} in the stiffness tensor $C^{\mathrm{ZB}}_{(111)}$, Eq. (14). In other words, we are left with a polarization vector equivalent to the WZ polarization vector $\mathbf{P}^{\mathrm{WZ,FO}}_{\mathrm{pz}}$ given in Eq. (26) and the strain field arising from

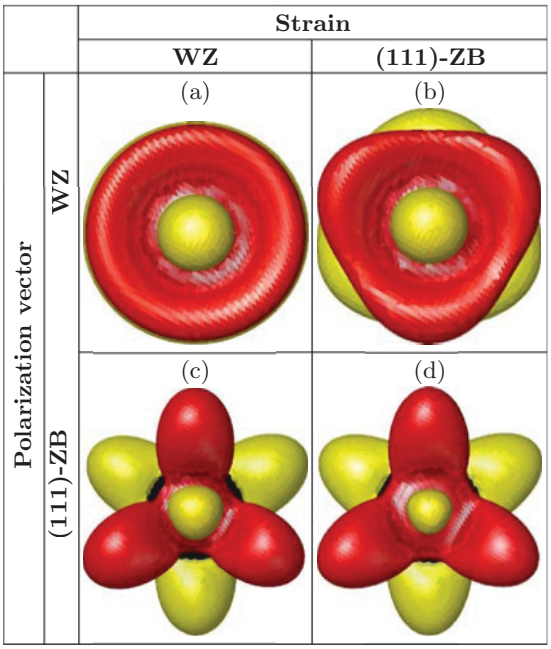

FIG. 7. (Color online) Comparison of the piezoelectric built-in potentials (first order) ϕ^{FO} in a (111)-oriented lens-shaped InGaAs/GaAs for different levels of approximation. (a) WZ-like approximation ($C'_{15}=0$, $e'_{11}=e'_{12}=0$), (b) shows the result for $C'_{15}\neq 0$ but $e'_{11}=e'_{12}=0$, (c) displays ϕ^{FO} for $C'_{15}=0$ but $e'_{11}\neq 0$ and $e'_{12}\neq 0$, and (d) is the full calculation ($C'_{15}\neq 0, e'_{11}\neq 0, e'_{12}\neq 0$). The red (dark gray) and yellow (light gray) isosurfaces correspond to +4 mV and −4 mV, respectively.

the elastic energy equivalent to $F_{\mathrm{WZ}}^{(0001)}$ in Eq. (8). Note that even though we use here the WZ-like approximation, the required elastic constants and piezoelectric coefficients are calculated from the cubic InAs and GaAs ones via Eqs. (15) and the expressions below Eq. (27). The built-in potential in this WZ-like approximation is denoted by ϕ_p^{eWZpWZ}, and is shown in Fig. 7(a). As expected, ϕ_p^{eWZpWZ} is equivalent to the piezoelectric built-in potential in WZ nitride-based QDs grown along the polar c axis.[20,84] The major difference between the built-in potential in the WZ-like approximation for the (111)-ZB InGaAs/GaAs system and a real III-N WZ system is that the potential drop along the growth direction is much larger in a realistic nitride system. This is linked to the fact that first the piezoelectric coefficients in the nitride system are several times larger compared to the "conventional" III-V systems and second that the total polarization also includes the spontaneous polarization contribution in the WZ system.

In a second step we study the impact of the strain field on the first-order built-in potential. Figure 7(b) shows the potential ϕ_p^{eZBpWZ}, taking the full stiffness tensor $C_{(111)}^{\mathrm{ZB}}$, Eq. (14), and therefore the strain field originating from the elastic energy $F_{\mathrm{ZB}}^{(111)}$, Eq. (16), into account. For the polarization vector we still apply the WZ-like approximation, Eq. (26). The calculated ϕ_p^{eZBpWZ} exhibits a C_{3v} symmetry instead of the $C_{\infty v}$ symmetry as observed in the WZ-approximation [cf. Fig. 7(a)]. However, the potential drop along the growth direction is unchanged by the change in the strain-field symmetry, as can be inferred from Fig. 8. Furthermore, one finds that even though the

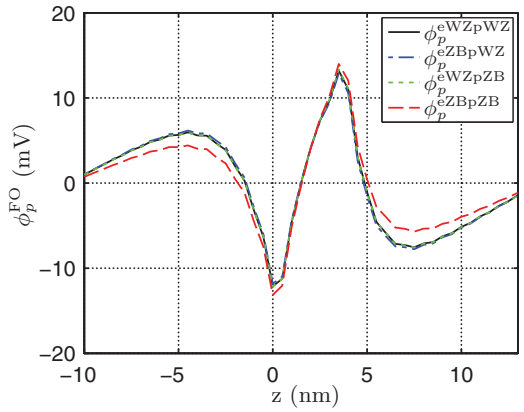

FIG. 8. (Color online) Electrostatic built-in potential ϕ_p^{FO} for a line scan through the center of a (111)-oriented lens-shaped InGaAs/GaAs QD along the [111] direction for different levels of approximation. The WZ-like approximation ($C'_{15}=0, e'_{11}=e'_{12}=0$) is denoted by ϕ_p^{eWZpWZ}, while ϕ_p^{eZBpWZ} shows the result for $C'_{15}\neq 0$ but $e'_{11}=e'_{12}=0$. The resulting built-in potential for $C'_{15}=0$ but $e'_{11}\neq 0$ and $e'_{12}\neq 0$ is given by ϕ_p^{eWZpZB} and the full calculation ($C'_{15}\neq 0, e'_{11}\neq 0, e'_{12}\neq 0$) by ϕ_p^{eZBpZB}.

strain field is obtained from the elastic energy $F_{\mathrm{ZB}}^{(111)}$ given by Eq. (16), which leads to a C_{3v} symmetry in ϕ_p^{eZBpWZ}, inside the QD ϕ_p^{eZBpWZ} is still very similar to ϕ_p^{eWZpWZ} in the WZ-like approximation. This is shown in Fig. 9(a) for a contour plot of the built-in potential at the base of the lens-shaped $In_{0.35}Ga_{0.65}As$ QD. The lower half shows ϕ_p^{eWZpWZ} while the upper half depicts ϕ_p^{eZBpWZ} based on the correct (111)-ZB strain field. The main differences between the two results starts to appear at the boundaries of the nanostructure. All in all, these results indicate that the actual symmetry of the strain field, for example $C_{\infty v}$ instead of C_{3v}, is only of secondary importance for the shape and the magnitude of the built-in potential inside the QD. Strain calculations for WZ nanostructures, based on harmonic continuum elasticity, should therefore be sufficient to gain insights in the behavior and the shape of the corresponding built-in potentials, even though the correct C_{3v} symmetry is not taken into account. Furthermore, when calculating the electronic structure of WZ nitride QDs, the single-particle

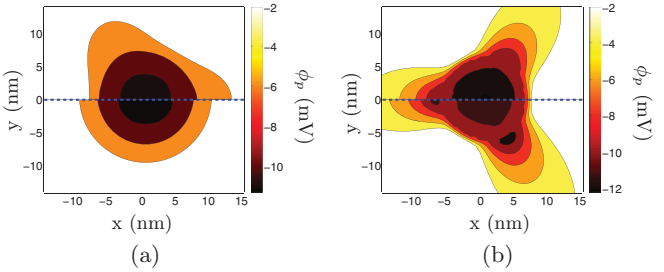

FIG. 9. (Color online) Contour plot of the first-order built-in potential ϕ_p^{FO} in the x-y plane, (111)-plane, at the base of lens-shaped (111)-oriented InGaAs/GaAs QD for different levels of approximation. The lower half in (a) shows ϕ_p^{eWZpWZ} while the upper half displays ϕ_p^{eZBpWZ}. In (b) the lower half depicts ϕ_p^{eWZpZB} and the upper half shows ϕ_p^{eZBpZB}. More details on ϕ_p^{α} are given in the caption of Fig. 8.

ground-state wave functions for electrons and holes are well localized inside the nanostructure due to the large band offsets in the nitride systems.[43] Therefore the built-in field calculated from a continuum-elasticity strain field, which neglects the C_{3v} symmetry of the underlying lattice, should have almost the same impact on these states and therefore on the emission wavelength as a built-in field based on a strain field showing the correct C_{3v} symmetry. We have recently used this assumption (including isotropic elastic constants) to derive a surface-integral approach to calculate the polarization potential.[85]

In a third step of investigating the potential, we analyze the influence of the additional terms e'_{11} and e'_{12} in $e^{\mathrm{ZB}}_{(111)}$, Eq. (27), on the first-order built-in potential compared to a WZ-like system, Eq. (25). Figure 7(c) shows the built-in potential ϕ_p^{eWZpZB} under the assumption of a WZ-like strain field, Eq. (8), but this time applying the full (111)-ZB first-order polarization vector $\mathbf{P}^{(111),\mathrm{FO}}_{\mathrm{pz}}$, Eq. (29). Comparing ϕ_p^{eWZpZB} with ϕ_p^{eZBpWZ} [cf. Fig. 7(b)], the C_{3v} symmetry in ϕ_p^{eWZpZB} is far more pronounced; however, the potential profile along the central axis through the center of the QD is unaffected by the change in the polarization vector, as shown in Fig. 8.

In the final step of our analysis of the first-order built-in potential, we employ the full first-order piezoelectric vector $\mathbf{P}^{(111),\mathrm{FO}}_{\mathrm{pz}}$ and the full elastic energy $F^{(111)}_{\mathrm{ZB}}$ to calculate ϕ_p^{eZBpZB}. The calculated built-in potential ϕ_p^{eZBpZB} is shown in Fig. 7(d). Again, when comparing ϕ_p^{eWZpZB} to ϕ_p^{eZBpZB}, the correct description of the C_{3v} symmetry of the strain field changes the potential slightly near the interfaces of the nanostructure. The line scan of the built-in potential along the growth direction and through the QD center is now slightly modified by the change in strain and piezoelectric constants, as shown in Fig. 8: small changes in the potential can be seen above and below the nanostructure. Similar changes are also visible when plotting the behavior of ϕ_p^{eZBpZB} in the (111) plane (x-y plane) compared to ϕ_p^{eWZpZB}, as depicted in Fig. 9(b).

D. Second-order piezoelectric polarization in (111)-zinc-blende structures

To obtain the second-order piezoelectric polarization vector $\mathbf{P}^{(111),\mathrm{SO}}_{\mathrm{pz}}$ in the (111)-oriented system, we apply, according to Eq. (11), the transformation

$$P^{(111),\mathrm{SO}}_{\mathrm{pz},i} = \sum_{\alpha} U_{i\alpha} P^{(001),\mathrm{SO}}_{\mathrm{pz},\alpha}, \tag{30}$$

where $\mathbf{P}^{(001),\mathrm{SO}}_{\mathrm{pz}}$ is the second-order piezoelectric polarization vector in the (001) system defined in Eq. (24). Equation (30) yields

$$\mathbf{P}^{(111),\mathrm{SO}}_{\mathrm{pz}} = 2A_1 \mathrm{Tr}(\epsilon') \begin{pmatrix} \sqrt{\frac{2}{3}} K_x \\ \sqrt{2} K_y \\ \sqrt{\frac{1}{3}} K_z \end{pmatrix} + 2A_2 \begin{pmatrix} \sqrt{\frac{2}{3}} [C_1(K_z - K_x) + C_2 K_y] \\ \sqrt{2}[C_2 C_3 + C_1 K_y] \\ \sqrt{\frac{1}{3}} [2C_1 K_x + 2C_2 K_y] \end{pmatrix} + 4B_{156} \begin{pmatrix} \sqrt{\frac{2}{3}} \left[K_y^2 - C_3 K_x\right] \\ \sqrt{2}[-K_y C_4] \\ \sqrt{\frac{1}{3}} \left[C_3(K_z - K_x) - K_y^2\right] \end{pmatrix}, \tag{31}$$

with

$$K_x = \frac{1}{2}(\epsilon'_{22} - \epsilon'_{11}) - \frac{1}{\sqrt{2}}\epsilon'_{13},$$
$$K_y = \frac{1}{\sqrt{3}}\epsilon'_{12} - \frac{1}{\sqrt{6}}\epsilon'_{23},$$
$$K_z = \epsilon'_{33} - \frac{1}{2}(\epsilon'_{22} + \epsilon'_{11}),$$
$$C_1 = \frac{1}{4}(\epsilon'_{22} - \epsilon'_{11}) + \frac{1}{\sqrt{2}}\epsilon'_{13},$$
$$C_2 = \sqrt{\frac{3}{2}}\epsilon'_{23} + \frac{\sqrt{3}}{2}\epsilon'_{12},$$
$$C_3 = \frac{1}{3}(\epsilon'_{33} - \epsilon'_{11}) - \frac{1}{3\sqrt{2}}\epsilon'_{13},$$

and

$$C_4 = \frac{1}{6}\epsilon'_{11} - \frac{1}{2}\epsilon'_{22} + \frac{1}{3}\epsilon'_{33} + \frac{\sqrt{2}}{3}\epsilon'_{13}.$$

Figure 10(a) shows the corresponding second-order piezoelectric built-in potential $\phi_p^{(111),\mathrm{SO}}$ in the (111)-oriented lens-shaped $In_{0.35}Ga_{0.65}As/GaAs$ QD, which we have used as a model system so far. The total built-in potential $\phi_p^{(111),\mathrm{total}}$ ($\phi_p^{(111),\mathrm{SO}} + \phi_p^{(111),\mathrm{FO}}$) is displayed in Fig. 10(b). As expected from our analysis of the first-order contribution $\phi_p^{(111),\mathrm{FO}}$,

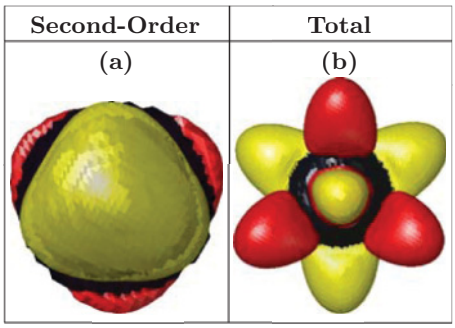

FIG. 10. (Color online) Comparison of the second-order ϕ_p^{SO} (a) and total built-in potential ϕ_p^{total} (b) (111)-oriented lens-shaped InGaAs/GaAs QD. In (a) the red (dark) and yellow (light) isosurfaces correspond to 2 mV and −2 mV, respectively, while in (b) red (dark gray) and yellow (light gray) isosurfaces correspond to 4 mV and −4 mV, respectively.

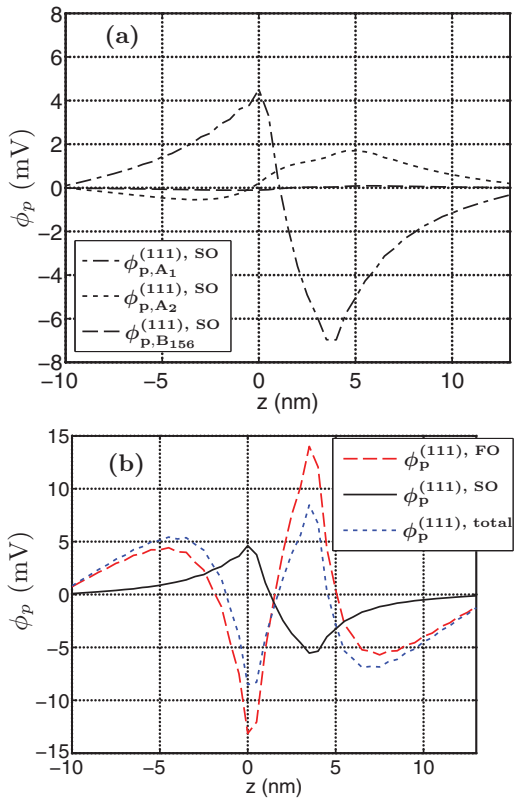

FIG. 11. (Color online) Built-in potential of a lens-shaped (111)-oriented ZB InGaAs/GaAs QD for a line scan through the center of the QD along the [111] direction (z axis). (a) The different contributions to the second-order built-in potential. $\phi^{(111),SO}_{p,A_1}$ (dashed dotted line) denotes the contribution arising from the A_1 related terms, $\phi^{(111),SO}_{p,A_2}$ (dotted line) originates from the A_2 terms while stems $\phi^{(111),SO}_{p,B_{156}}$ (dashed) from B_{156} in Eq. (31). (b) The different contributions to the total piezoelectric potential $\phi^{(111),total}_p$ (dotted line). The first-order contribution is denoted by $\phi^{(111),FO}_p$ (dashed line) while $\phi^{(111),SO}_p$ (solid line) is the second-order term.

$\phi^{(111),SO}_p$ exhibits also a C_{3v} symmetry. However, and in contrast to $\phi^{(111),FO}_p$, the second-order contribution does not change sign outside the QD and is largest in magnitude at the top and the bottom of the nanostructure. Furthermore, the potential $\phi^{(111),SO}_p$ shows a different orientation and a different sign at the interfaces between QD and surrounding material compared to $\phi^{(111),FO}_p$ [cf. Fig. 7(d)].

To analyze the second-order built-in potential $\phi^{(111),SO}_p$ in more detail, we now consider separately the three different terms in Eq. (31) related to A_1 ($\phi^{(111),SO}_{p,A_1}$), A_2 ($\phi^{(111),SO}_{p,A_2}$), and B_{156} ($\phi^{(111),SO}_{p,B_{156}}$), respectively. Figure 11(a) shows a line scan through the center of the QD along the [111] direction of the potential due to each of the three terms. Based on the currently available second-order piezoelectric constants A_1, A_2, and B_{156}, the A_1-related contribution clearly dominates the second-order built-in potential. The contribution arising from A_2 is only of secondary importance, while the B_{156} term is negligible along the central QD axis. The full second-order piezoelectric built-in potential $\phi^{(111),SO}_p$ is shown in Fig. 11(b) together with the first-order potential $\phi^{(111),FO}_p$ and the total built-in potential $\phi^{(111),total}_p$, for the same line scan as in Fig. 11(a). The difference in sign between the first- and second-order built-in potential contributions is clearly seen in Fig. 11(b). Similar to the (001) system, as discussed, for example, in Ref. 69, the second-order contribution $\phi^{(111),SO}_p$ is mainly localized inside the QD, while $\phi^{(111),FO}_p$ spreads considerably into the surrounding barrier material. This is related to the strain-field dependence of the two contributions. The first-order polarization vector $\mathbf{P}^{(111),FO}_{pz}$, Eq. (29), is a function of shear strain components and sums and differences of diagonal terms ϵ_{ii} of the strain tensor. In contrast, the second-order polarization vector $\mathbf{P}^{(111),SO}_{pz}$, Eq. (31), is mainly determined by products of diagonal and shear strain components. Since the diagonal components ϵ_{ii} are largest inside the nanostructure and near the boundaries, $\mathbf{P}^{(111),SO}_{pz}$ has a significant contribution in this region only. Therefore the total built-in potential $\phi^{(111),total}_p$ outside the QD is mainly determined by the first-order contribution $\phi^{(111),FO}_p$, as shown in Fig. 11. Inside the nanostructure, due to opposite signs, first- and second-order terms tend to cancel each other. This could then lead to a field-free QD, as, for example, discussed in Refs. 56 and 69 for (001)-oriented lens-shaped InGaAs/GaAs QDs. However, as shown by Schliwa *et al.* for (001)-oriented ZB systems[69] and recently also for (111)-oriented structures,[13] the balance between first- and second-order contributions is very sensitive to the QD shape, size, and composition.

Therefore the analysis of the experimental data on high-quality site-controlled QDs in combination with theoretical studies should be very promising to shed light on the description of nonlinear piezoelectric effects in ZB semiconductor nanostructures.

V. CONCLUSION

In summary, we have derived expressions for the stiffness tensor and the elastic energy in (111)-ZB systems along with equations for first- and second-order piezoelectric polarization vectors in these structures. These equations allow for an efficient calculation of strain and piezoelectric fields in (111)-oriented ZB nanostructures, such as site-controlled (111)-oriented InGaAs/GaAs QDs, which are most promising candidates for entangled photon sources.

Moreover, the chosen approach offers the possibility to gain access to the key parameters, which modify, for example, strain and piezoelectric fields in (111)-oriented ZB heterostructures compared to conventional (001) systems. Additionally, since the two structures are very similar, the comparison of (111)-ZB and (0001)-WZ structures is beneficial for both systems. On the one hand, this comparison allows us to split the expressions derived in the (111)-ZB system into a WZ-like component and contributions which are related to the differences between the two systems. These differences lead to extra terms in different quantities of the (111)-oriented ZB system, which are not present in a WZ system. More specifically, we find here that the (111)-ZB elastic tensor contains an additional off-diagonal elastic constant C'_{15}, which has no analog in the WZ tensor. This extra off-diagonal term shows an angle dependence in the (111) plane and modifies therefore the elastic energy in a (111)-ZB system compared to a WZ-like

system. We have shown here that this in-plane angle dependence of C'_{15} leads to modifications in the calculated strain field when using a continuum-based approach, with these changes being relatively small but relevant to symmetry considerations in our prototypical (111)-oriented ZB dot. In particular, our analysis of the strain field in a (111)-oriented lens-shaped InGaAs/GaAs QD shows the correct C_{3v} symmetry when taking the C'_{15}-related terms in the elastic energy into account. In the WZ-like approximation ($C'_{15} = 0$), the symmetry is $C_{\infty v}$, introduced by the lens-shaped QD geometry.

Additionally, we have shown that the first-order piezoelectric tensor in (111)-ZB systems contains contributions that are not present in a c-plane WZ system. Similar to the discussion of the strain field, these terms lead to a C_{3v} symmetry in the resultant first-order built-in potential, instead of a $C_{\infty v}$ symmetry in WZ approximation, with these terms having a strong effect on the in-plane variation in potential.

In addition to providing insight into the key factors that modify strain and built-in fields in (111)-oriented ZB heterostructures, our approach offers, furthermore, the opportunity to gain insights into material parameters for the WZ AlN, InN, and GaN systems. For example, the sign of the shear strain related piezoelectric constant e_{15} is still under debate in WZ nitrides. From our analysis of the first-order piezoelectric tensor in the (111)-ZB system we obtain that the piezoelectric coefficients e_{31} and e_{15} should be equal and negative, and that the ratio $e_{33}/e_{31} = -2$. When comparing these ratios with ratios derived from literature piezoelectric coefficients, we find a very good agreement for GaN and InN and a good agreement for AlN, as long as the literature value of e_{15} is negative. From this we conclude that e_{15} should be negative in WZ nitrides.

ACKNOWLEDGMENTS

This work was carried out with the financial support of Science Foundation Ireland. S.S. was further supported by the IRCSET Embark Initiative.

APPENDIX

As detailed by Fedorov[86] the minimum number of invariants that are required to describe the elastic tensor is not necessarily achieved using the crystallographic axes as a reference frame. For tetragonal and rhombohedral crystals Blanchfield and Saunders[87] discussed that when the reference frame is appropriately chosen, the number of required elastic constants can be reduced. Blanchfield and Saunders[87] derived, after a rotation by an angle ϕ around the z axis, the following expressions for the components of the elastic stiffness tensor:

$$\begin{aligned}
\bar{C}_{11} &= \bar{C}_{22} = \tilde{C}_{11} + C\cos(4\phi) + C_{16}\sin(4\phi),\\
\bar{C}_{66} &= \tilde{C}_{66} - C\cos(4\phi) - C_{16}\sin(4\phi),\\
\bar{C}_{12} &= \tilde{C}_{12} - C\cos(4\phi) - C_{16}\sin(4\phi),\\
\bar{C}_{16} &= -\bar{C}_{26} = -C\sin(4\phi) + C_{16}\cos(4\phi),\\
\bar{C}_{14} &= -\bar{C}_{24} = C_{14}\cos(3\phi) + C_{25}\sin(3\phi),\\
\bar{C}_{56} &= C_{14}\cos(3\phi) + C_{25}\sin(3\phi),\\
\bar{C}_{25} &= -\bar{C}_{15} = -C_{14}\sin(3\phi) + C_{25}\cos(3\phi),\\
\bar{C}_{46} &= -C_{14}\sin(3\phi) + C_{25}\cos(3\phi),\\
\bar{C}_{33} &= C_{33},\\
\bar{C}_{44} &= \bar{C}_{55} = C_{44},\\
\bar{C}_{13} &= \bar{C}_{23} = C_{13},\\
\bar{C}_{34} &= \bar{C}_{35} = \bar{C}_{45} = \bar{C}_{36} = 0,
\end{aligned} \tag{A1}$$

with

$$C = \tfrac{1}{4}(C_{11} - C_{12} - 2C_{66}), \tag{A2}$$

$$\tilde{C}_{11} = C_{11} - C, \tag{A3}$$

$$\tilde{C}_{66} = C_{66} + C, \tag{A4}$$

and

$$\tilde{C}_{12} = C_{12} + C. \tag{A5}$$

To obtain the elastic stiffness tensor of the (111)-oriented ZB system given in Eq. (14), we have used a specific set of basis vectors defining the rotation matrix U in Eq. (10). Following our discussions above, we study now the angle dependence of the elastic constants $\bar{C}_{ijkl}$ using Eqs. (A1). When using the elastic constants from Eq. (14), the coefficients given in Eqs. (A2)–(A5) reduce to

$$\begin{aligned}
C &= 0,\\
\tilde{C}_{11} &= C'_{11},\\
\tilde{C}_{66} &= C'_{66},\\
\tilde{C}_{12} &= C'_{12}.
\end{aligned}$$

Therefore, with Eqs. (A1), the elastic constants $\bar{C}_{ijkl}$ take the form

$$\begin{aligned}
\bar{C}_{11} &= \bar{C}_{22} = C'_{11},\\
\bar{C}_{66} &= C'_{66},\\
\bar{C}_{12} &= C'_{12},\\
\bar{C}_{16} &= -\bar{C}_{26} = 0,\\
\bar{C}_{14} &= -\bar{C}_{24} = \bar{C}_{56} = -C'_{15}\sin(3\phi),\\
\bar{C}_{25} &= -\bar{C}_{15} = \bar{C}_{46} = -C'_{15}\cos(3\phi),\\
\bar{C}_{33} &= C'_{33},\\
\bar{C}_{44} &= \bar{C}_{55} = C'_{44},\\
\bar{C}_{13} &= \bar{C}_{23} = C'_{13},\\
\bar{C}_{34} &= \bar{C}_{35} = \bar{C}_{45} = \bar{C}_{36} = 0.
\end{aligned}$$

This yields

$$\bar{C} = \begin{pmatrix} C'_{11} & C'_{12} & C'_{13} & -C'_{15}\sin(3\phi) & C'_{15}\cos(3\phi) & 0 \\ C'_{12} & C'_{11} & C'_{13} & C'_{15}\sin(3\phi) & -C'_{15}\cos(3\phi) & 0 \\ C'_{13} & C'_{13} & C'_{33} & 0 & 0 & 0 \\ -C'_{15}\sin(3\phi) & C'_{15}\sin(3\phi) & 0 & C'_{44} & 0 & -C'_{15}\cos(3\phi) \\ C'_{15}\cos(3\phi) & -C'_{15}\cos(3\phi) & 0 & 0 & C'_{44} & -C'_{15}\sin(3\phi) \\ 0 & 0 & 0 & -C'_{15}\cos(3\phi) & -C'_{15}\sin(3\phi) & C'_{66} \end{pmatrix}, \tag{A6}$$

with $C'_{66} = \frac{1}{2}(C'_{11} - C'_{12})$. From this we conclude the following: First, the specific form for the elastic stiffness tensor $C^{\mathrm{ZB}}_{(111)}$ in a (111)-oriented ZB system depends on the chosen set of basis vectors and therefore on the transformation matrix U. Second, the additional terms in the elastic tensor $C^{\mathrm{ZB}}_{(111)}$ compared to the WZ system Eq. (7), show a threefold symmetry according to the discussion above [cf. Eq. (A6)]. Consequently, the calculated strain field shown in the upper half of Fig. 3 exhibits a C_{3v} symmetry.

[1] P. Michler, *Single Quantum Dots: Fundamentals, Applications, and New Concepts*, Topics in Applied Physics (Springer, Berlin, 2000), Vol. 90.

[2] D. Bimberg, M. Grundmann, and N. N. Ledentsov, *Quantum Dot Heterostructures* (Wiley, Chichester, 2001).

[3] O. Benson, C. Santori, M. Pelton, and Y. Yamamoto, Phys. Rev. Lett. **84**, 2513 (2000).

[4] N. Akopian, N. H. Lindner, E. Poem, Y. Berlatzky, J. Avron, D. Gershoni, B. D. Gerardot, and P. M. Petroff, Phys. Rev. Lett. **96**, 130501 (2006).

[5] E. Knill, R. Laflamme, and G. J. Milburn, Nature (London) **409**, 46 (2001).

[6] K. J. Resch, J. S. Lundeen, and A. M. Steinberg, Phys. Rev. Lett. **89**, 037904 (2002).

[7] A. Shields, Science **297**, 1821 (2002).

[8] G. Bester, S. Nair, and A. Zunger, Phys. Rev. B **67**, 161306(R) (2003).

[9] R. Seguin, A. Schliwa, S. Rodt, K. Potschke, U. W. Pohl, and D. Bimberg, Phys. Rev. Lett. **95**, 257402 (2005).

[10] R. Seguin, A. Schliwa, T. D. Germann, S. Rodt, K. Pötschke, A. Strittmatter, U. W. Pohl, D. Bimberg, M. Winkelnkemper, T. Hammerschmidt *et al.*, Appl. Phys. Lett. **89**, 263109 (2006).

[11] A. Rastelli, A. Ulhaq, S. Kiravittaya, L. Wang, A. Zrenner, and O. Schmidt, Appl. Phys. Lett. **90**, 073120 (2007).

[12] R. Singh and G. Bester, Phys. Rev. Lett. **103**, 063601 (2009).

[13] A. Schliwa, M. Winkelnkemper, A. Lochmann, E. Stock, and D. Bimberg, Phys. Rev. B **80**, 161307 (2009).

[14] E. Pelucchi, S. Watanabe, K. Leifer, Q. Zhu, B. Dwir, P. D. L. Rios, and E. Kapon, Nano Lett. **7**, 1282 (2007).

[15] Q. Zhu, K. F. Karlsson, E. Pelucchi, and E. Kapon, Nano Lett. **7**, 2227 (2007).

[16] L. O. Mereni, V. Dimastrodonato, R. J. Young, and E. Pelucchi, Appl. Phys. Lett. **94**, 223121 (2009).

[17] V. Dimastrodonato, L. O. Mereni, G. Juska, and E. Pelucchi, Appl. Phys. Lett. **97**, 072115 (2010).

[18] A. Mohan, M. Felici, P. Gallo, B. Dwir, A. Rudra, J. Faist, and E. Kapon, Nature Photonics **4**, 302 (2010).

[19] S. B. Healy, R. J. Young, L. O. Mereni, V. Dimastrodonato, E. Pelucchi, and E. P. O'Reilly, Physica E (Amsterdam) **42**, 2761 (2010).

[20] D. P. Williams, S. Schulz, A. D. Andreev, and E. P. O'Reilly, J. Sel. Top. Quant. Electron. **15**, 1092 (2009).

[21] S. Schulz and E. P. O'Reilly, Phys. Status Solidi A **208**, 1551 (2011).

[22] A. E. Romanov, T. J. Baker, S. Nakamura, and J. S. Speck, J. Appl. Phys. **100**, 023522 (2006).

[23] S. Muensit, E. M. Goldys, and I. L. Guy, Appl. Phys. Lett. **75**, 3965 (1999).

[24] F. Bernardini and V. Fiorentini, Appl. Phys. Lett. **80**, 4145 (2002).

[25] M. Feneberg, F. Lipski, R. Sauer, K. Thonke, T. Wunderer, B. Neubert, P. Brückner, and F. Scholz, Appl. Phys. Lett. **89**, 242112 (2006).

[26] K. Tsubouchi and M. Mikoshiba, IEEE Trans. Sonics Ultrason. **32**, 634 (1985).

[27] G. Bu, D. Ciplys, M. Shur, L. J. Schowalter, S. Schujman, and R. Gaska, Appl. Phys. Lett. **84**, 4611 (2004).

[28] H. Shen, M. Wraback, H. Zhong, A. Tyagi, S. P. DenBaars, S. Nakamura, and J. S. Speck, Appl. Phys. Lett. **95**, 033503 (2009).

[29] S. Schulz, A. Berube, and E. P. O'Reilly, Phys. Rev. B **79**, 081401(R) (2009).

[30] S. Founta, F. Rol, E. Bellet-Amalric, J. Bleuse, B. Daudin, B. Gayral, H. Mariette, and C. Moisson, Appl. Phys. Lett. **86**, 171901 (2005).

[31] C.-Y. Yeh, Z. W. Lu, S. Froyen, and A. Zunger, Phys. Rev. B **46**, 10086 (1992).

[32] G. F. Koster, J. O. Dimmock, R. G. Wheeler, and H. Statz, *Properties of thirty-two point groups* (M. I. T. Press, Massachusetts, 1969).

[33] G. Bester and A. Zunger, Phys. Rev. B **71**, 045318 (2005).

[34] N. Baer, S. Schulz, P. Gartner, S. Schumacher, G. Czycholl, and F. Jahnke, Phys. Rev. B **76**, 075310 (2007).

[35] F. Widmann, J. Simon, B. Daudin, G. Feuillet, J. L. Rouvière, N. T. Pelekanos, and G. Fishman, Phys. Rev. B **58**, R15989 (1998).

[36] M. Senes, K. L. Smith, T. M. Smeeton, S. E. Hooper, and J. Heffernan, Phys. Rev. B **75**, 045314 (2007).

[37] L. D. Landau and E. M. Lifshitz, *Theory of Elasticity* (Pergamon, Oxford, U. K., 1986).

[38] M. Povolotskyi, A. Auf der Maur, and A. Di Carlo, Phys. Status Solidi C **2**, 3891 (2005).

[39] D. Barettin, S. Madsen, B. Lassen, and M. Willatzen, Superlattices Microstruct. **47**, 134 (2010).

[40] C. Pryor, J. Kim, L. W. Wang, A. J. Williamson, and A. Zunger, J. Appl. Phys. **83**, 2548 (1998).

[41] J. F. Nye, *Physical Properties of Crystals: Their Representation by Tensors and Matrices* (Oxford University Press, New York, 1985).
[42] F. Bechstedt, U. Grossner, and J. Furthmüller, Phys. Rev. B **62**, 8003 (2000).
[43] I. Vurgaftman and J. R. Meyer, J. Appl. Phys. **94**, 3675 (2003).
[44] K. Shimada, Jpn. J. Appl. Phys. **45**, L358 (2006).
[45] J. M. Hinckley and J. Singh, Phys. Rev. B **42**, 3546 (1990).
[46] R. W. Martin, Phys. Rev. B **6**, 4546 (1972).
[47] M. E. Sherwin and T. J. Drummond, J. Appl. Phys. **69**, 8423 (1991).
[48] [www.sphinxlib.de].
[49] O. Marquardt, S. Boeck, C. Freysoldt, T. Hickel, and J. Neugebauer, Comput. Phys. Commun. **181**, 765 (2010).
[50] S. Boeck, C. Freysoldt, A. Dick, L. Ismer, and J. Neugebauer, Comput. Phys. Commun. **182**, 543 (2011).
[51] P. Bhattacharya, ed., *Properties of Lattice-Matched and Strained Indium Gallium Arsenide* (INSPEC, London, 1993).
[52] M. Schulz, U. Rössler, and O. Madelung, eds., *Numerical Data and Functional Relationships in Science and Technology*, Vol. III/17a of *Landolt-Börnstein: Condensed matter* (Springer, Berlin, 1982).
[53] S. Adachi, *Physical Properties of III-V Semiconductor Compounds: InP, InAs, GaAs, GaP, InGaAs and InGaAsP* (Wiley Interscience, New York, 1992).
[54] G. Bester, X. Wu, D. Vanderbilt, and A. Zunger, Phys. Rev. Lett. **96**, 187602 (2006).
[55] W. G. Cady, *Piezoelectricity* (McGraw-Hill, New York, 1946).
[56] G. Bester, A. Zunger, X. Wu, and D. Vanderbilt, Phys. Rev. B **74**, 081305(R) (2006).
[57] F. Bernardini, V. Fiorentini, and D. Vanderbilt, Phys. Rev. B **56**, R10024 (1997).
[58] F. Bernardini, V. Fiorentini, and D. Vanderbilt, Phys. Rev. B **63**, 193201 (2001).
[59] M. Willatzen, B. Lassen, L. L. Y. Voon, and R. V. N. Melnik, J. Appl. Phys. **100**, 024302 (2006).
[60] U. M. E. Christmas, A. D. Andreev, and D. A. Faux, J. Appl. Phys. **98**, 073522 (2005).
[61] S. A. Dickey, A. Majerfeld, J. L. Sánchez-Rojas, A. Sacedón, E. Muñoz, A. Sanz-Hervás, M. Aguilar, and B. W. Kim, Microelectron. Eng. **43-44**, 171 (1998).
[62] S. Cho, A. Majerfeld, A. Sanz-Hervás, J. J. Sánchez, J. L. Sánchez-Rojas, and I. Izupra, J. Appl. Phys. **90**, 915 (2001).
[63] J. J. Sánchez, J. I. Izupra, J. M. G. Tijero, E. Muñoz, S. Cho, and A. Majerfeld, J. Appl. Phys. **91**, 3002 (2002).
[64] S. P. Łepkowski, Phys. Rev. B **77**, 155327 (2008).
[65] P. Ballet, P. Disseix, J. Leymarie, A. Vasson, A.-M. Vasson, and R. Grey, Phys. Rev. B **59**, R5308 (1999).
[66] M. A. Migliorato, D. Powell, A. G. Cullis, T. Hammerschmidt, and G. P. Srivastava, Phys. Rev. B **74**, 245332 (2006).
[67] L. C. Lew Yan Voon and M. Willatzen, J. Appl. Phys. **109**, 031101 (2011).
[68] M. Ediger, G. Bester, A. Badolato, P. M. Petroff, K. Karrai, A. Zunger, and R. J. Warburton, Nature Physics **3**, 774 (2007).
[69] A. Schliwa, M. Winkelnkemper, and D. Bimberg, Phys. Rev. B **76**, 205324 (2007).
[70] V. Mlinar and A. Zunger, Phys. Rev. B **79**, 115416 (2009).
[71] W. Zhang, M. Gong, C.-F. Li, G.-C. Guo, and L. He, J. Appl. Phys. **106**, 104314 (2009).
[72] P. G. McDonald, J. Shumway, and I. Galbraith, Appl. Phys. Lett. **97**, 173101 (2010).
[73] S. Muensit and I. L. Guy, Appl. Phys. Lett. **72**, 1896 (1998).
[74] T. Takeuchi, H. Amano, and I. Akasaki, Jpn. J. Appl. Phys. **39**, 413 (2000).
[75] K. Shimada, T. Sota, and K. Suzuki, J. Appl. Phys. **84**, 4951 (1998).
[76] I. L. Guy, S. Muensit, and E. M. Goldys, Appl. Phys. Lett. **75**, 4133 (1999).
[77] A. Zoroddu, F. Bernardini, P. Ruggerone, and V. Fiorentini, Phys. Rev. B **64**, 045208 (2001).
[78] A. Al Yacoub and L. Bellaiche, Appl. Phys. Lett. **79**, 2166 (2001).
[79] A. Dal Corso, M. Posternak, R. Resta, and A. Baldereschi, Phys. Rev. B **50**, 10715 (1994).
[80] J. G. Gualtieri, J. A. Kosinski, and A. Ballato, IEEE Trans. Ultrason. Ferroelectr. Freq. Control **41**, 53 (1994).
[81] C. M. Lueng, H. L. W. Chan, C. Surya, and C. L. Choy, J. Appl. Phys. **88**, 5360 (2000).
[82] To obtain the e_{ij} coefficients in the case that only the piezoelectric strain/modulus constants d_{ij} are given, we use the expression $e_{31} = d_{33}C_{13} + d_{31}(C_{11} + C_{12})$, $e_{33} = d_{33}C_{33} + d_{31}2C_{13}$ and $e_{15} = d_{15}C_{44}$, derived from the equations given in Ref. 44.
[83] M. Murayama and T. Nakayama, Phys. Rev. B **49**, 4710 (1994).
[84] D. P. Williams, A. D. Andreev, E. P. O'Reilly, and D. A. Faux, Phys. Rev. B **72**, 235318 (2005).
[85] S. B. Healy and E. P. O'Reilly, J. Phys.: Conf. Ser. **245**, 012022 (2010).
[86] F. I. Fedorov, *Theory of elastic waves in crystals* (Plenum Press, New York, 1968).
[87] P. Blanchfield and G. A. Saunders, J. Phys. C **12**, 4673 (1979).